Taming Distributed One-Hop Multicasting in Millimeter-Wave VANETs

Jiangang Shen, *Member, IEEE*, Hongzi Zhu, *Member, IEEE*, Yunxiang Cai, *Member, IEEE*, Shan Chang, *Member, IEEE*, Haibin Cai, *Member, IEEE*, Bangzhao Zhai, *Member, IEEE*, Xudong Wang, *Fellow, IEEE*, and Minyi Guo, *Fellow, IEEE*

***Abstract*—Efficient one-hop multicasting (OHM) of high-volume sensor data plays a pivotal role in the success of cooperative autonomous driving applications. Although millimeter-Wave (mmWave) bands demonstrate huge potential for high-bandwidth OHM data transmission, the challenge lies in enabling individual vehicles to locate and communicate with suitable neighbors in a fully distributed and highly dynamic scenario. This paper introduces mmV2V, a fully distributed OHM scheme designed for vehicular networks, comprising three tightly integrated protocols. Initially, synchronized vehicles perform a probabilistic neighbor discovery procedure, wherein randomly divided transmitters (or receivers) clockwise scan (or listen to) the surroundings in synchronization with heterogeneous Tx (or Rx) beams. This approach facilitates the identification of the vast majority of neighbors within a few repeated rounds. Subsequently, vehicles engage in negotiations with their neighbors to establish an optimal communication schedule in evenly distributed slots. Finally, matched pairs of neighboring vehicles commence high data rate transmissions using refined beams. We implement a prototype testbed to validate the feasibility of the main components of mmV2V. Extensive simulations based on generated and real-world traffic traces are conducted and the results demonstrate that mmV2V consistently achieves a high completion ratio in demanding OHM tasks across various traffic conditions.**

***Index Terms*—Beamforming, mmWave communication, neighbor discovery, one-hop multicasting, vehicular networks.**

I. Introduction

As NEW vehicles are seeking higher levels of driving automation, more sophisticated sensors such as LIDAR and high-resolution cameras are equipped on such vehicles [1]. The data rate of sensory data generated by a self-driving vehicle can be up to 750 Mbps [2] and perception fusion methods like early-fusion and deep-fusion which help vehicles achieve more robust perception of surrounding environments require for large amount of raw data and feature exchange between one-hop neighboring vehicles [3], [4], [5]. Traditional communication protocol working in low frequency band like 802.11p cannot undertake such heavy load. There is an urgent need for new V2V communication technology with higher bandwidth so that huge amount of sensory data can be exchanged among neighboring vehicles in real time [6], [7], [8]. As millimeter-wave (mmWave) bands in 60 GHz have about 14 GHz unlicensed spectrum, current 5 G standards have introduced mmWave bands (FR2) for high data rate communication [9]. Moreover, mmWave bands also exhibit a great potential for future V2V communications. We focus on the *one-hop multicasting* (OHM) problem in mmWave vehicular networks, i.e., vehicles need to constantly exchange high-volume sensory data with their one-hop neighbors with narrow mmWave wireless beams. Fig. 1 illustrates an OHM scenario, where vehicles equipped with LIDAR exchange their individual 3D point cloud data with each of their one-hop neighbors via directional mmWave beams.

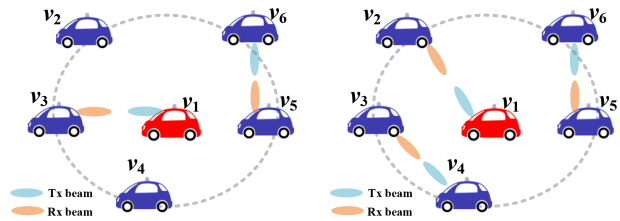

(a) Sub-optimal schedule example (b) Optimal schedule example

Fig. 1. Illustration of mmWave vehicular network, where data transmission only happens when a Tx beam is aligned with a Rx beam. In the OHM problem, each vehicle (e.g., v_1) needs to individually communicate with its one-hop neighbors (e.g., vehicles within the dotted disk area). Without centralized coordination, the network throughput may be sub-optimal as shown in (a) due to an inappropriate schedule.

A practical OHM protocol in mmWave vehicular networks should satisfy three rigid requirements as follows. First, the protocol should fit in fully distributed settings due to the possible lack of a central unit such as a road side unit (RSU). Second, considering the characteristics of directional mmWave links, the protocol should maximize the number of aligned transmitter-and-receiver pairs and the corresponding link quality to achieve

Manuscript received 29 September 2023; revised 21 February 2024; accepted 15 March 2024. Date of publication 26 March 2024; date of current version 3 October 2024. This work was supported in part by the National Natural Science Foundation of China under Grant 61972081, in part by the Natural Science Foundation of Shanghai under Grant 22ZR1400200, in part by the STIC under Grant CJGJZD20210408092400001, and in part by the Fundamental Research Funds for the Central Universities. Recommended for acceptance by J. Rodrigues. *(Corresponding author: Hongzi Zhu.)*

Jiangang Shen, Hongzi Zhu, Yunxiang Cai, and Minyi Guo are with the Department of Computer Science and Engineering, Shanghai Jiao Tong University, Shanghai 200240, China (e-mail: hongzi@sjtu.edu.cn).

Bangzhao Zhai and Xudong Wang are with UM-SJTU Joint Institute, Shanghai Jiao Tong University, Shanghai 200240, China.

Shan Chang is with the School of Computer Science and Technology, Donghua University, Shanghai 201620, China.

Haibin Cai is with Software Engineering Institute, East China Normal University, Shanghai 200241, China.

Digital Object Identifier 10.1109/TMC.2024.3381955

supreme network throughput. Last but not least, the protocol should be resilient to high mobility of vehicles which requires fast and frequent beam realignment.

In the literature, several pilot studies have demonstrated the feasibility of mmWave V2X communications. Wang et al. [2] deploy an experimental testbed consisting of one vehicle and four RSUs to enable microscopic investigation of the channel and the V2R link. Kim et al. [10] evaluate the performance of 802.11ad for V2V communication using a pair of vehicles. Such recent studies mainly focus on link-level measurements and have not considered the overall performance of the whole network. In traditional mmWave networks, plenty of beam alignment schemes between multiple clients and Access Points (APs) have been proposed to increase the network throughput and robustness. BounceNet [11] is the first many-to-many mmWave beam alignment protocol that can exploit dense spatial reuse to allow many AP-to-client links to operate in parallel in a confined space and scale the wireless throughput with the number of clients. mmChoir [12] is a proactive blockage mitigation technique that utilizes joint transmissions from multiple APs to provide blockage resilience to clients. These protocols are designed for indoor scenarios and require centralized APs, which cannot be applied to fully distributed vehicular environments. As a result, there is no existing distributed protocol, to the best of our knowledge, that can successfully address the OHM problem in mmWave vehicular networks.

In this paper, we propose a fully distributed scheme, called *mmV2V*, which can effectively tackle the OHM problem in mmWave vehicular networks. The core idea of mmV2V is for individual vehicles to first efficiently discover their neighbors with directional Tx or Rx beams. More specifically, vehicles are synchronized and randomly choose to clockwise scan or listen to the surroundings in unison. Then, to determine an optimal neighbor to communicate, vehicles negotiate with their neighbors in evenly distributed time slots scheduled with a common hash function. Finally, an agreed pair of neighboring vehicles start to communicate with refined beams. The process repeats until a vehicle has exchanged data with all its neighbors.

There are two main challenges to be solved when designing mmV2V. First, the neighborhood of a vehicle is rapidly changing and hard to identify only with mmWave beams. Uncoordinated attempts from individual vehicles would only arouse signal collisions and unaligned beams. In mmV2V, vehicles are first synchronized via the Global Positioning System (GPS) and then conduct a probabilistic neighbor discovery procedure, consisting of multiple independent rounds. In each round, all vehicles can recognized one half of their neighbors without interfering with each other by letting all Tx and Rx beams scan in pace but with a 180° offset. As a result, after a small number of K rounds, a large ratio of $1-0.5^K$ neighbors can be identified. In addition, heterogeneous beam widths are used for Tx and Rx beams, respectively, to obtain an optimal discovery efficiency.

Second, in a fully distributed setting, it is very challenging for individual vehicles to collectively make a communication schedule that maximizes the whole network throughput. Indeed, to determine the optimal communication schedule is NP-hard even if the global network information is available. In order to tackle this challenge, mmV2V leverages a novel distributed greedy algorithm. In this algorithm, each vehicle negotiates about the optimal communication schedule with each of its neighbor according to a negotiation sequence of slots. The sequence is determined with a common hash function so that the same pair of neighbors are arranged to the identical slot but different pairs of neighbors are arranged to distinct slots. As a result, vehicles are coordinated to exchange and update their individual decisions util they meet consensus after a few negotiation slots.

We implement a 60 GHz prototype testbed, consisting of two experiment vehicles, to verify the feasibility of main components of mmV2V. It requires minimal hardware requirements and is a fully distributed protocol. In our implementation, the neighbor discovery scheme can always identify a neighbor in a correct beam alignment configuration with at least 9.7 dB gain. Furthermore, we also verify the channel and beam pattern model with our real-world signal-to-noise ratio (SNR) trace. The efficacy of beam refinement is also verified in our experiment. We conduct large-scale simulations where each vehicle performs a data exchange task requiring 200 Mbps data rate with its neighbors in various scenarios with different traffic densities. In normal traffic condition, mmV2V can complete 74.7% of the task, in contrast to 31.9% and 46.5% achieved by a random scheme and IEEE 802.11ad, respectively. The results demonstrate the efficacy of mmV2V design. We highlight the main contributions in this paper as follows: 1) the OHM problem in mmWave vehicular networks is proposed; 2) a probabilistic neighbor discovery scheme without signal collisions is proposed; 3) a distributed greedy communication scheduling algorithm is proposed; 4) a 60 GHz prototype testbed is implemented and extensive simulations are conducted, demonstrating the efficacy of mmV2V.

II. System Model and Problem Definition

A. System Model

We consider more practical and challenging situation where there is no centralized control unit available. Vehicles move at variable speeds in the same direction on multi-lane surface roads and have equal capabilities as stated below:

- *Communication:* Each vehicle is equipped with a 60 GHz mmWave radio and a phased antenna array which can beam the signal with a desired beam width and in a desired direction according to multi-level codebooks. A co-channel deployment, uniform transmission power and half-duplex mode are assumed. V2V communications are operated under time division duplexing (TDD).
- *Synchronization:* Vehicles are synchronized through GPS receivers which can achieve high synchronization accuracy of less than 100 ns [13], [14]. In addition, vehicles can also obtain their heading direction information with GPS receivers.
- *Computation:* Vehicles can perform basic calculations such as modulo operation and random number generation.

B. Problem Definition

Without the loss of generality, we consider those vehicles that have line-of-sight (LOS) path within the communication range of a vehicle v_i as its one-hop neighbors, denoted as $\mathcal{N}_i$. The OHM problem is to determine a communication schedule such that the total time consumption for each vehicle $v_i \in V$ to exchange its sensory data with all its one-hop neighbors $v_j \in \mathcal{N}_i$ is minimized. Given that time is divided into synchronized slots for all vehicles, we give the formal definition of OHM problem as follows:

$$\begin{aligned} & \min\{\,|T|\,\} \\ \text{s.t.} \quad & \sum_{v_j \in \mathcal{N}_i} l_{i,j}^t \le 1,\ \forall v_i \in V,\ \forall t \in T, \\ & \sum_{t=0}^{|T|-1} \sum_{v_j \in \mathcal{N}_i} l_{i,j}^t \cdot d_{i,j}^t = D_{i,j},\ \forall v_i \in V, \end{aligned} \tag{1}$$

where T is the set of required time slots and $|T|$ is the number of time slots in T; $l_{i,j}^t$ denotes the communication state between v_i and v_j in time slot t, i.e., $l_{i,j}^t = 1$ means v_i communicate with v_j at time slot t and $l_{i,j}^t = 0$ means v_i and v_j do not communicate with each other at time slot t; $d_{i,j}^t$ denotes the amount of data exchanged between v_i and v_j in time slot t and $D_{i,j}$ represents the total amount of data to be transferred between v_i and v_j. Based on the definition of OHM problem, we have the following theorem:

Theorem 1: *The OHM problem is NP-hard.*

Proof: Let $\mathcal{G} = \langle V, E \rangle$ denote the vehicular network, where $V = \{v_i, 1 \le i \le N\}$ is the set of vehicles and $E = \{l_{ij}, i \ne j\}$ is the set of LOS links between a pair of neighboring vehicles v_i and v_j. We simplify the OHM problem by assuming $D_{i,j}$ is all the same for arbitrary pair of vehicles v_i and v_j and can be exchanged within one time slot t. We also assume that each vehicle v_i knows $\mathcal{G}$. With these assumptions, if we utilize one color to represent one time slot, the OHM problem is equal to find a schedule which can assign the minimum number of colors to all edges in E without assigning one color to any two or more edges connecting the same vehicle. This is the classic edge coloring problem which has been proved to be NP-complete [15]. In a fully distributed setting, the OHM is even harder because it is difficult for each individual vehicle to obtain the global network information (e.g., the location information of each vehicle in the network) and coordinate with each other. This concludes the proof.

III. Design of mmV2V

A. Overview

In mmV2V, synchronized vehicles exchange their data in independent beacons. In a beacon, as illustrated in Fig. 2, all vehicles follow the same protocol, which consists of three components, i.e., synchronized neighbor discovery, distributed consensual matching, and unicast data transmission.

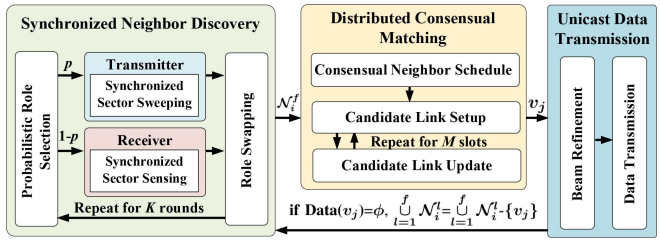

Fig. 2. Architecture of mmV2V.

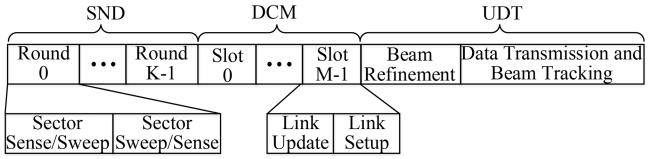

Fig. 3. Beacon structure of mmV2V.

Synchronized Neighbor Discovery (SND): SND consists of multiple discovery rounds. In each round, a vehicle v_i first probabilistically selects a role as a transmitter or as a receiver. Then, all transmitters start to clockwise sweep the surroundings (divided into equal sectors) with wide transmission beams, and meanwhile all receivers start to sense on the corresponding opposite sector with wide reception beams. With this synchronized beam sweeping and sensing procedure, each receiver can efficiently collect the link information from those LOS transmitters without collisions. After that, vehicles swap their roles and conduct the synchronized beam sweeping and sensing procedure again. As a result, both ends of a LOS link make acquaintance to each other. With high probability, vehicle v_i can identify the vast majority of neighbors in the fth beacon, denoted as $\mathcal{N}_i^f$, after a few number of discovery rounds.

Distributed Consensual Matching (DCM): Given all identified neighbors, DCM consists of a sequence of negotiation slots, during which each vehicle try to find the optimal neighbor for data transmission. In a distributed network setting, individual vehicles first perform the consensual neighbor schedule (CNS) that uses a Hash function to distribute neighboring vehicle pairs into different time slots to avoid packet collisions. In each slot, a vehicle v_i exchanges the information of its current candidate with the neighbor v_j designated by the CNS. If v_j is a better candidate in terms of maximizing the network throughput, v_i and v_j respectively set each other as their new candidates and update this change with their previous candidates.

Unicast Data Transmission (UDT): After consensual matching, vehicle v_i has determined which neighbor v_j to exchange data with. To obtain optimal data transmission rate, v_i and v_j conduct fast beam refinement to search for the best narrow beam alignment, only within the range of the corresponding wide beam previously used for neighbor discovery. Then, they exchange a unit of data using the refined beams in the remaining time of this beacon. If all sensory data have been exchanged with v_j, v_i removes v_j from $\cup_{l=1}^{f} \mathcal{N}_i^l$. After that, v_i repeats the whole

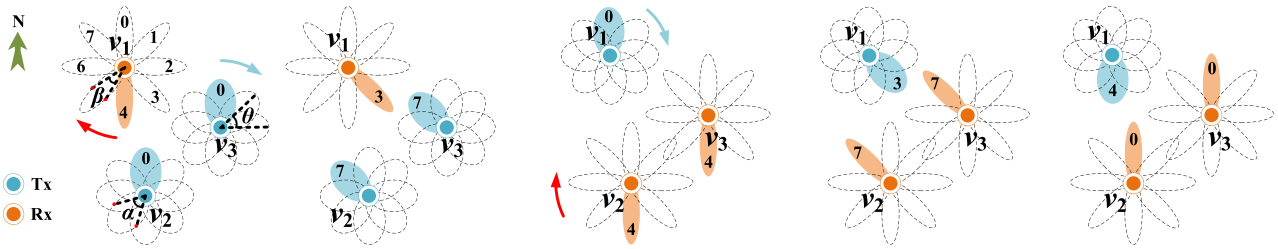

(a) Initial state, v_1 is roughly aligned with v_2 (b) v_1 is roughly aligned with v_3 (c) The state after role swapping (d) v_3 is roughly aligned with v_1 (e) v_2 is roughly aligned with v_1

Fig. 4. Snapshots in an example of one synchronized neighbor discovery round, where v_1 selects to be a receiver and v_2 and v_3 select to be transmitters.

process of mmV2V protocol until all sensory data have been exchanged with all its neighbors.

B. Synchronized Neighbor Discovery

In a fully distributed mmWave vehicular network, a vehicle needs to acquire precise location information of its neighboring vehicles, in order to conduct beam alignment for better link condition. However, it is challenging to efficiently identify neighbors only with non-broadcasting mmWave radios. In mmV2V, neighbor discovery is coordinated among vehicle without being interfered with each other. Specifically, neighbor discovery consists of K rounds and time complexity of SND is $O(KS)$ where S is the number of predefined sectors. In each round, a vehicle v_i performs a sequence of operations elaborated as follows:

1) Probabilistic Role Selection: Vehicle v_i first selects a role as a transmitter with the probability of p or as a receiver with the probability of $1-p$. Given the independent role selection among vehicles, the whole network is expected to be separated with evenly distributed $N \cdot p$ transmitters and $N \cdot (1-p)$ receivers, where N is the number of vehicles in the network.

2) Synchronized Sector Sweeping: After role selection, all transmitters are synchronized to clockwise sweep on a set of S predefined sectors with beams of α degrees wide measured at 3 dB attenuation. Sectors are indexed from the north direction, ranging from 0 to $S-1$, and the interval of two consecutive sectors $\theta = 360^\circ/S$. When sweeping on a sector, a transmitter sends out a sweep frame, consisting of its ID (e.g., MAC address) and the sector ID information. As illustrated in Fig. 4(a), v_2 and v_3 select to be transmitters and their surroundings are equally divided into $S = 8$ sectors, with Sector 0 pointing at the north. Guided by the direction obtained from GPS receivers, v_2 and v_3 start to sweep from Sector 0 to Sector 7.

3) Synchronized Sector Sensing: Similarly, after role selection, all receivers are synchronized to clockwise sense on the same set of S predefined sectors but from the south sector (i.e., the opposite sector of the north sector), with beams of β wide. In general, if the current sweeping sector ID is i, the sensing sector ID is $(i + \frac{S}{2})\%S$. When sensing a sector, a receiver passively listen from the reception beam. As illustrated in Fig. 4(a), v_1 selects to be a receiver and starts to sense on Sector 4 (i.e., the opposite sector of Sector 0). In this case, v_1 is roughly aligned with v_2 and can obtain v_2's ID, sweeping sector ID and the channel SNR information. With this synchronized sector sweeping and sensing scheme, all receivers can obtain the link information with all their LOS transmitters. For instance, as depicted in Fig. 4(b), v_1 gets to know about v_3 when the sweeping sector ID is seven and the sensing sector ID is three.

4) Role Swapping: After all sectors are swept or sensed, all vehicles swap their roles, i.e., a transmitter becomes a receiver and vice versa, and respectively do the synchronized sector sweeping and sensing again. For example in Fig. 4(c), v_1 starts to sweep from Sector 0 and v_2 and v_3 start to sense from Sector 4. In this way, the LOS link information can be obtained by both ends of the link. For instance in Fig. 4(c) and (d), v_3 and v_2 also know about the LOS link with v_1, respectively. Algorithm 1 shows the pseudo code of SND.

It should be noted that the settings of width of sweeping beams α and that of sensing beams β are a tradeoff between neighbor discovery efficiency and accuracy. With wider beams, the sweeping and sensing process consumes less time but coarser link measurement can be obtained. Moreover, with high probability, each vehicle can identify the vast majority of neighbors after a few number of discovery rounds. We have the following observation:

Observation: If vehicles in the network use the same probability p to select a role, then $p = 0.5$ can make a vehicle identify the maximum number of LOS neighbors; after K discovery rounds, the expected ratio of identified neighbors is $1 - 0.5^K$ for $p = 0.5$.

Proof: For a vehicle v_i, as each vehicle individually selects its role, we consider the probability of one neighboring vehicle to be discovered without loss of generality. A neighboring vehicle that cannot be identified by v_i after K discovery rounds is the vehicle that choose exactly the same roles as v_i for K times. Therefore, the probability for that to happen is $f(p,K) = [p^2 + (1-p)^2]^K$. To minimize $f(p,K)$, we have $\frac{df(p,K)}{dp} = 0$ which leads to $p = 0.5$. After K discovery rounds, the expected ratio of identified neighbors is $1 - [p^2 + (1-p)^2]^K$, which is $1 - 0.5^K$ for $p = 0.5$ and concludes the proof. ■

C. Distributed Consensual Matching

Given all identified neighbors, as stated in Theorem 1, the OHM problem is NP-hard. Without global network topology information, it is even harder for each vehicle to choose an optimal neighbor to communicate so that the whole network

Algorithm 1: Procedure of SND for v_i.

Input: Tx beam width α_0, Rx beam width β_0, the number of sectors S_0

Initialize discovered one-hop neighbor set $\mathcal{N}_i^f \leftarrow \{\}$
for $k \in 0, 1, .., K-1$ **do**
  Generate a random number $p \in [0, 1]$
  if p>0.5 **then**
    SWEEP(α_0, S_0)
    SENSE($\beta_0, S_0, \mathcal{N}_i^f$)
  else
    SENSE($\beta_0, S_0, \mathcal{N}_i^f$)
    SWEEP(α_0, S_0)
Function SWEEP (α, S)
  Set beamwidth to α
  for $k \in 0, 1, .., S-1$ **do**
    Send a sweep frame to sector k
Function SENSE ($\beta, S, \mathcal{N}_i^f$)
  Set beamwidth to β
  for $k \in \frac{S}{2}\%S, (\frac{S}{2}+1)\%S, .., (\frac{S}{2}+S-1)\%S$ **do**
    Listen on sector k
    if *Receive a sweep frame from* v_j **then**
      $\mathcal{N}_i^f.append(v_j)$

throughput is maximized. In mmV2V, each vehicle negotiates with its neighbors in M continuous slots and time complexity of DCM is $O(M)$. The detailed two-step negotiation process is stated as follows.

1) Consensual Neighbor Schedule: To avoid two or more neighboring vehicles simultaneously negotiating with the same vehicle, each vehicle arranges a negotiation sequence of M slots. For vehicle v_i, it schedules vehicle $v_j \in \mathcal{N}_i^f$ to the kth slot if $(H(MAC(v_i)) + H(MAC(v_j)))\%C = k\%C$, for $k \in [0, M-1]$, where $H(\cdot)$ is a Hash function; $MAC(\cdot)$ returns the MAC address of a vehicle; and C is a constant used to separate vehicles in $\mathcal{N}_i^f$ into different slots. For example, as illustrated in Fig. 5(a), we assume that v_2 has a LOS path with v_1 and v_3, respectively, and $M = 3, C = 3, (H(MAC(v_1)) + H(MAC(v_2)))\%3 = 2$ and $(H(MAC(v_2)) + H(MAC(v_3)))\%3 = 0$. In this case, v_1 and v_2 will both schedule each other to Slot 2, and v_2 and v_3 will both schedule each other to Slot 0.

Note that when M is larger than C, vehicle $v_j \in \mathcal{N}_i^f$ can be arranged in v_i's sequence for multiple times. The purpose of this is for both vehicles to update their decisions (see below). If there are more than one vehicles in $\mathcal{N}_i^f$ being assigned to the same slot due to Hash collision or a small C, v_i will random pick one to fill the slot.

2) Candidate Link Setup and Update: Vehicle v_i negotiates with its neighbors one by one according to the determined negotiation sequence. Specifically, in each slot, if there is a vehicle $v_j \in \mathcal{N}_i^f$ is scheduled in that slot, v_i and v_j will exchange the link quality information of their current communication candidates.[1] Both vehicles will set each other as the new communication candidate if one of the following conditions stands: 1) both v_i and v_j have no candidates; 2) v_i (or v_j) has a candidate v_l but the quality of the link between v_i and v_j is better than the candidate link between v_i (or v_j) and v_l. Otherwise, v_i and v_j keep their current candidates unchanged. In addition, for the second condition, v_i (or v_j) will also update with v_l to inform v_l that v_i (or v_j) is no longer its candidate. The pseudo code of DCM is shown in Algorithm 2.

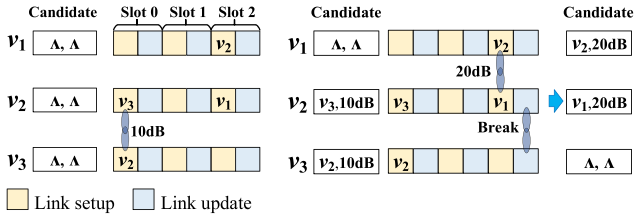

(a) v_2 and v_3 mutually setup a candidate link with each other

(b) v_2 setups a new link with v_1 and break the previous link with v_3

Fig. 5. Illustration of distributed consensual matching, where v_2 has a LOS path with v_1 and v_3, respectively and $M = 3, C = 3$.

For example in Fig. 5(a), in Slot 0, both v_2 and v_3 have no current candidate. After exchange this information, both vehicles record each other as the current candidate and the SNR of the link (e.g., 10 dB) as shown in the left part of Fig. 5(b). In Slot 2, as the quality of the link between v_2 and v_1 (e.g., 20 dB) is better than that of the link between v_2 and v_3, v_2 changes its candidate from v_3 to v_1 and informs v_3 with this change during the second half of Slot 2, as shown in the right part of Fig. 5(b).

Although the whole matching process lasts for predefined M slots, we prove that the matching process converges in finite slots.

Theorem2: DCM converges in finite slots.

Proof: $E = \{l_{ij}, i \neq j\}$ is the set of LOS links between a pair of neighboring vehicles v_i and v_j. As DCM seeks for better link quality, the best link in E will be established and will not break after a finite m negotiation slots since the number of neighbors of a vehicle is finite. Without loss of generality, we assume the best link is $l_{i,j}$ between v_i and v_j. Then we can remove all links related to v_i and v_j from E as v_i and v_j is a fixed pair. The above phase will be repeated until $E = \{\}$ and this is the final state of DCM which can be achieved in a finite number of negotiation slots as E is a finite set. This concludes the proof.

D. Unicast Data Transmission

After distributed consensual matching, a vehicle v_i has determined which neighbor v_j is optimal to exchange data with. However, v_i and v_j are coarsely aligned with wide beams. To further obtain better data transmission rate, v_i and v_j conduct beam refinement to search for the best alignment with the narrowest beams. Specifically, as illustrated in Fig. 6, the number of narrowest beams needed to search on each side is $s = \lfloor \frac{\theta}{\theta_{\min}} \rfloor + 1$,

[1] Both vehicles follow a rule to transmit their information in turn. For example, the vehicle with a larger MAC address does first.

Algorithm 2: Procedure of DCM for v_i.

Input: Constant C, the number of negotiation slots M, identified one-hop neighbor set $\mathcal{N}_i^f$

Initialize negotiation set $\mathcal{N}_i^c \leftarrow \{\}$, candidate $c_i \leftarrow NULL$
for $k \in 0, 1, .., M-1$ **do**
  $flag \leftarrow False$
  $\mathcal{N}_i^c \leftarrow \{\}$
  for $v_j \in \mathcal{N}_i^f$ **do**
    if $(H(MAC(v_i)) + H(MAC(v_j)))\%C = k\%C$ **then**
      $\mathcal{N}_i^c.append(v_j)$
  LINKSETUP($flag, \mathcal{N}_i^c, c_i$)
  LINKUPDATE($flag, c_i$)
Function LINKSETUP ($flag, \mathcal{N}_i^c, c_i$)
  Random select a v_j from $\mathcal{N}_i^c$
  // $q_{i,j}$ is the link quality between v_i and v_j
  if *($c_i == c_j == NULL$) or ($q_{i,j}$ is the best)* **then**
    $flag \leftarrow True$
    $c_i \leftarrow v_j$
Function LINKUPDATE ($flag, c_i$)
  if $flag == True$ **then**
    Send previous candidate v_k with break message
  else
    if *Receive break message from* c_i **then**
      $c_i \leftarrow NULL$

where θ is the sector interval as stated in Section III-B2 and $\theta_{\min}$ is the interval of narrow beams. As s is usually very small, v_i and v_j find the best narrow beam alignment via cross searching. Finally, they exchange a unit of data with the refined narrowest beams. To maintain the optimal link quality on move, v_i and v_j will conduct Extended Kalman Filter (EKF) based beam tracking [16] during data transmission.

IV. Prototype Implementation

We implement a 60 GHz prototype testbed consisting of two experiment vehicles to verify the beam pattern model we used in large-scale simulations and the synchronized sector sweep and beam refinement in mmV2V. Specifically, both vehicles are synchronized with COTS GPS modules, which can achieve low synchronization errors of less than 1 ms measured under all urban scenarios in Shanghai city. Each vehicle has a USRP N210 software defined radio [17] equipped with LFTX and LFRX daughterboards, and a Sivers IMA EVK06002 platform [18]. The configuration of the experiment vehicle is illustrated in Fig. 7 and the block diagram of hardware connection is illustrated in Fig. 8, where the USRP N210 is used to process Tx and Rx baseband signals, and the EVK06002 platform is used as the mmWave RF front-end and mounted on the roof of the vehicle.

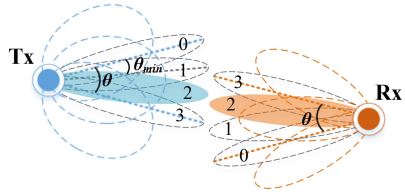

Fig. 6. Illustration of beam refinement, where the optimal narrow beams can be aligned via cross searching.

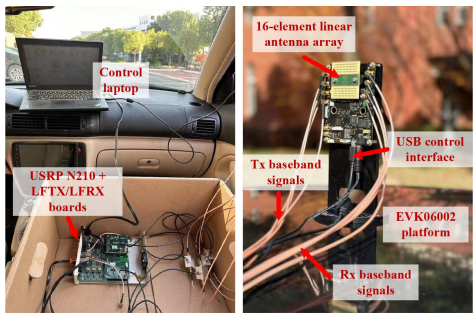

Fig. 7. Configuration of the experiment vehicle in our prototype testbed.

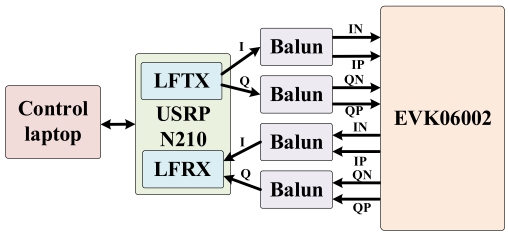

Fig. 8. Block diagram of hardware connection.

The central frequency of our testbed is set to 60.48 GHz. We use a 16-element linear phased array from the EVK06002 platform, where each antenna is equipped with a 6-bit phase-shifter. The predefined codebook of a EVK06002 platform contains 63 beams with main lobes ranging from -45° to $+45^\circ$ at angles. The interval of two consecutive sectors θ is set to 15°. With our prototype hardware configuration, it takes 8 ms to switch a beam and the duration of a sweep frame is set to 2 ms with the first 1 ms for enduring synchronization errors and the rest 1 ms for data transmission. Therefore, it takes 200 ms and 600 ms to finish one round of neighbor discovery and the whole SND with three neighbor discovery rounds, respectively. As in our experiments vehicles can always find each other at the correct sector and match, we mainly focus on validating the physical layer of mmV2V in our experiments.

First, we verify utilize the beam pattern utilized in our simulations. The beam pattern is based on a 3GPP channel model [19], which defines the antenna gain at orientation γ as

$$g^a(\gamma) = \begin{cases} g^1 10^{-\frac{3}{10}(\frac{|\gamma|}{\omega/2})^2} & |\gamma| < \theta_1 \\ g^2 & \theta_1 < |\gamma| < \pi \end{cases}, \quad (2)$$

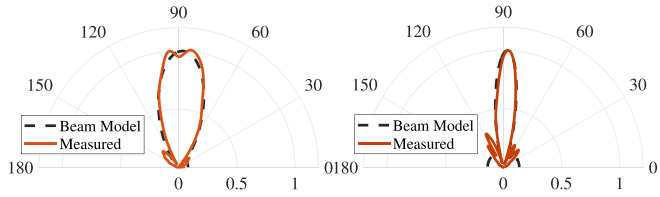

Fig. 9. Beam utilized in synchronized sector sweep.

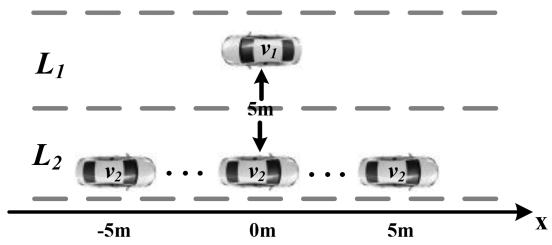

Fig. 10. Illustration of field experiment scenario.

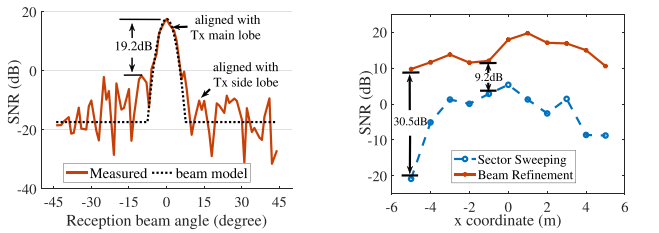

(a) SNR measured during sector sweeping

(b) Maximum SNR measured during sector sweeping and beam refinement

Fig. 11. SNR measured in our field study.

where ω is the 3 dB beam width; g^1 and g^2 are the main lobe gain and side lobe gain, respectively; and $\theta_1 = \omega/2\sqrt{10/3\log_{10}(g^1/g^2)}$ is the boundary of the main lobe and the side lobe. Specifically, we utilize 4 and 8 antennas in the centre of phased array to beamform wide Tx and Rx beams, respectively. To measure the beam pattern, we fix one phased array and rotate the other from 0° to 180° with an interval of 3° and measure the signal strength on each direction. Fig. 9 plots the measured Tx beam pattern and RX beam pattern, the beam pattern of the 3GPP model is also plotted for comparison. It can be seen that the 3GPP beam pattern model can well capture the main characteristics of our linear phased array.

We then verify the synchronized sector sweeping and sensing in outdoor vehicular setting. As illustrated in Fig. 10, we stop both experiment vehicles v_1 (Tx) and v_2 (Rx) at each meter zero location of two adjacent lanes L_1 and L_2, respectively. The width of each lane is 5 meters. In this setting, vehicles conduct synchronized sector sweeping/sensing accordingly from $-45°$ to $+45°$ with an interval of $1.5°$ using fine beams formed with all 16 antennas. Fig. 11(a) plots the average SNR measured at receiver as a function of the reception beam angle. It can be seen that the SNR reaches the maximum when the reception beam is aligned with the main lobe of the transmission beam and drops as the reception beam angle increases. In addition, though SNR peaks can be seen when the reception beam aligns with side lobes of the transmission beam, they are about 19 dB lower than the maximum SNR, which means that the receiver can successfully identify the transmitter and the corresponding sector (or beam) ID. Moreover, the dotted black curve plotted in Fig. 11(a) is derived from the adopted beam pattern model.

Due the hardware limitation, we then verify the synchronized sector sweeping/sensing and the beam refinement schemes with v_2 at different fixed locations. Specifically, as illustrated in Fig. 10, we fix v_1 at meter zero in lane L_1, and let v_2 moves one meter forward and stops from meter -5 to meter 5 in lane L_2, respectively. For each location of v_2, v_1 first acts as transmitter and v_2 acts as receiver to conduct synchronized sector sweeping/sensing. After that, both vehicle swap their roles and repeat the process. Thereafter, v_1 and v_2 immediately conducts beam refinement with their Rx/Tx roles unchanged, using narrow beams formed with all 16 antennas. The sweeping range is set from $-5°$ to $+5°$ of the direction of the identified sector and the sweeping interval θ is set to $5°$. During the process, we measure the SNR at v_1. Fig. 11(a) plots the maximum SNR achieved during the synchronized sector sweeping and the beam refinement for each location of v_2. It can be seen that with beam refinement the link quality can be largely improved, the highest increase of SNR reaches 30.5 dB and even the least increase of SNR reaches 9.2 dB, demonstrating the efficacy of beam refinement.

V. Performance Evaluation

A. Methodology

We use VENUS [20], which is a vehicular network simulator supporting microscope transportation simulations, to generate road traffic of different density on a road segment of one kilometer long with three lanes of 5 meters wide on each direction. The speed range on three lanes is 40–60 km/h, 50–70 km/h, and 60–80 km/h, respectively. The simulator calculates the location of each vehicle based on a car-following model and a lane-changing model. In addition, we also evaluate mmV2V on a real-world trace, referred to as the *highD* dataset [21], in which more than 110,500 vehicle are recorded at six locations on German highways with a drone. The highD dataset consists of 60 recordings and each recording lasts for about 15 minutes. We randomly pick 5 clips from each recording and each clip lasts for 20 s in our experiments. Since the highD dataset only provides vehicle positions with a time granularity of 40 ms, we conduct linear interpolation between two consecutive vehicle positions to achieve vehicle trajectories with a time granularity of 5 ms.

We adopt the standard long-distance path loss model [22] in our simulations, which is formulated as

$$g^l_{i,j} = a \cdot 10 \cdot \log_{10} d + O + 15 \cdot d/1000, \tag{3}$$

where d is the distance between v_i and v_j; a represents the path loss exponent; O is a constant determined by the number of blockers; and the last term is atmospheric attenuation. We adopt the channel and beam pattern models defined in (2). Assume

v_j receives data from v_i, the SINR measured at v_j at time t is calculated as

$$SINR_{i,j}(t) = \frac{p_i(t)g_i^t(t)g_{i,j}^c(t)g_j^r(t)}{N_0B + \sum_{k\in N_j, k\neq i} p_k(t)g_k^t(t)g_{k,j}^c(t)g_j^r(t)} \quad (4)$$

where $p_i(t) = 28$ dBm is v_i's transmission power; $g_i^a(t)$ and $g_j^a(t)$ are antenna gain of v_i and v_j, respectively; $N_0 = -174$ dBm/Hz is the Gaussian noise power density; and $B = 2.16$ GHz is the bandwidth of the channel. We adopt the a set of Modulation and Coding Schemes (MCS) of IEEE 802.11ad protocol [23], i.e., from MCS0 to MCS12, which achieve different data transmission rates up to 4.62 Gbps according to the measured Error Vector Magnitude (EVM) calculated as $SINR^{-1/2}$ [24].

The duration of one beacon is set to 20 ms. The delay for forming a new beam is 1 μs [23] and the narrowest beam width is set to 10°. We use the 802.11ad Sector level Sweep (SSW) frame as our sweep frame when doing synchronized sector sweeping/sensing, which takes 15 μs [25]. To scan 24 sectors, one round of SND takes 0.8 ms. According to 802.11ad `aControlPHYPreambleLength` and `aSIFSTime`, the beacon delivery delay and the beacon processing delay are set to 4.3 μs and 3 μs, respectively. One negotiation slot in DCM takes 30 μs with 15 μs for candidate link setup and 15 μs for link update. Considering about channel dynamics caused by vehicle movement, vehicle position and link quality is updated every 5 ms which is within the coherence time [26] in our simulations.

We consider a typical application of 3GPP video data sharing for assisted and improved automated driving (VaD) [27], referred to as *high resolution image exchange* (HRIE) task, which requires 100-700 Mbps data rate for exchanging video data (with resolution 1280 x 720, 24 b per pixel, 30 fps).

We compare our neighbor discovery scheme with the Random Neighbor Discovery (RND) scheme [28], and compare our matching scheme with two schemes, i.e., the Simple Distributed Weighted Matching (SDWM) scheme [29] and a Random Matching (RM) scheme:

- *RND:* In this neighbor discovery scheme, each vehicle randomly selects a role (e.g., Tx or Rx) and a direction to cast a Tx or Rx beam. When a Tx beam is aligned with a Rx beam, the corresponding Tx vehicle is identified by the Rx vehicle.
- *SDWM:* In this matching scheme, vehicles have a second broadcasting channel to exchange information to all its neighbors. Each vehicle chooses the unmatched neighbor that has the best link quality with itself. A pair of vehicles are matched if they choose each other and they broadcast this information to their own neighbors.
- *RM:* In this matching scheme, each vehicle randomly selects a neighbor. A pair of vehicles are matched if they are both unmatched before and choose each other.

We compare the overall performance of mmV2V with the following two schemes:

- *Random OHM Protocol (ROP):* ROP adopts the RND and RM schemes for neighbor discovery and matching, respectively.
- *IEEE 802.11ad:* The PBSS (Personal Basic Service Set) of IEEE 802.11ad, where stations can communicate with each other directly, can be utilized for solving the OHM problem. In addition, a central unit called PCP (PBSS control point) is in charge of communication scheduling in a PBSS [30]. In our experiments, beacon length are set to be 20 ms and the probability that one vehicle chooses to be PCP is set to 30%. After receiving several beacons sent by PCPs, a vehicle will randomly choose a PBSS to join in.

We consider the following three metrics to evaluate the performance of all candidate schemes:

- *OHM Completion Ratio (OCR):* Let $\mathcal{N}_i^C$ denote the set of neighboring vehicles that have completed data exchange with v_i. OCR of v_i is calculated as $\frac{|\mathcal{N}_i^C|}{|\mathcal{N}_i|}$.
- *Average of Transmission Progress (ATP):* Let $D_{i,j}$ denote the amount of data that have exchanged between v_i and v_j, and let $\eta_{i,j}$ denote the transmission progress between v_i and v_j, i.e., $\eta_{i,j} = \frac{D_{i,j}}{D}$. ATP of v_i, denoted as $\overline{\eta_i}$, reflects the average progress of data exchange between v_i and its neighbors, calculated as $\overline{\eta_i} = \frac{1}{|\mathcal{N}_i|}\sum_{v_j\in\mathcal{N}_i}\eta_{i,j}$.
- *Deviation of Transmission Progress (DTP):* DTP of v_i is calculated as $\sqrt{\frac{\sum_{v_j\in\mathcal{N}_i}|\eta_{i,j}-\overline{\eta_i}|^2}{|\mathcal{N}_i|}}$, which measures the fairness of communication opportunities among its neighbors. A small DTP value means that v_i tends to exchange data with its neighbors equally.

B. Parameter Configuration

1) Effect of Beam Width α and β: In this experiment, we examine the effect of Tx and Rx beam width (α and β, respectively) to the performance of neighbor discovery. In line with the 802.11ad control message requirement that EVM is no larger than -6 dB, we consider a vehicle v_j that has a LOS path of no less than 6 dB SNR with v_i within 100 meters as a neighbor of v_i. We generate various traffic on the simulated 6-lane dual-direction road segment, with vehicle density varying from 15 vehicles per lane per kilometer (vpl) to 30 vpl with an interval of 5 vpl. In each traffic setting, we respectively vary α and β from 10° to 60° with an interval of 2° and set the sweeping and sensing interval $\theta = \frac{\alpha}{2}$ for one hundred times. We calculate the probability that a neighbor can be successfully identified with the SND protocol.

Fig. 12 plots the neighbor discovery probability under traffic scenarios, where the solid curves in each subfigure present the probability of 95% obtained under different combination of α and β. It can be seen that with narrow Tx and Rx beams, it is guaranteed to identify all neighbors in all traffic scenarios. However, the number of sector *S* is determined by Tx beam width and it will also take longer time using narrower Tx beams in one discovery round. It is therefore a tradeoff between neighbor discovery efficiency and accuracy. We set $\alpha = 30°$ and $\beta = 12°$ in the following experiments so that 95% neighbors can be efficiently discovered in all traffic conditions meanwhile the number of sectors is the minimum. In addition, it can also be seen that in general, the probability increases as the vehicle density

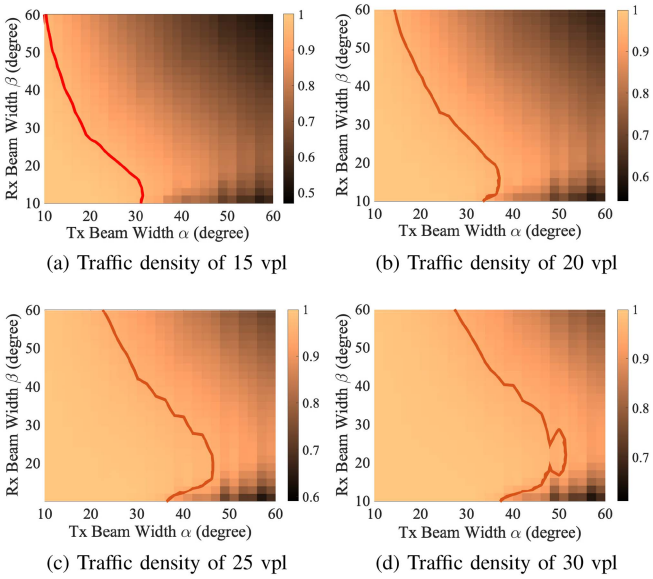

Fig. 12. Effect of Tx and Rx beam width in identifying neighbors under traffic of different densities.

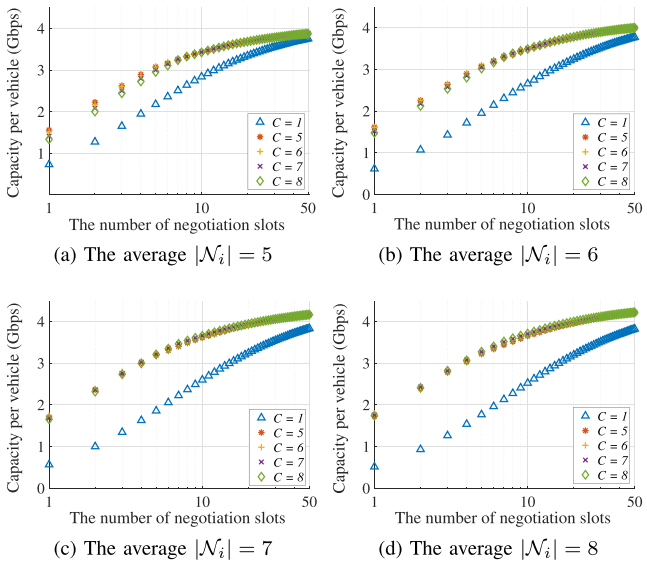

Fig. 13. Capability of the constant C to separate neighbors in different negotiation slots.

increases. It is because when vehicles are dense, the distance between a pair of neighbors is also short, which reduces the path loss.

2) Effect of the Constant C: In this experiment, we explore the capability of the constant C (and together the hash function) to separate neighbors in different negotiation slots. Similarly, we generate traffic of different densities. In each traffic setting, we vary the value of C from one to twelve with an interval of one, and calculate the average communication capacity per vehicle over the whole network after a certain number of negotiation slots.

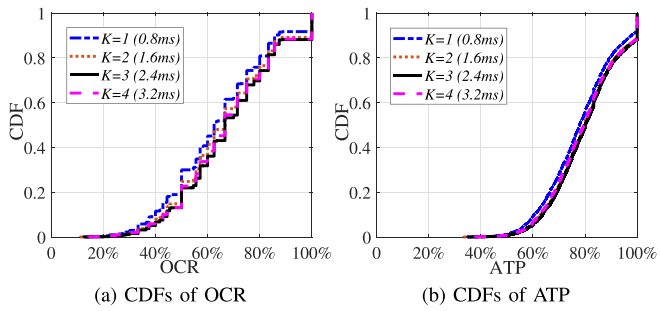

Fig. 14. Effect of the number of discovery trials K.

Fig. 13 plots the capacity per vehicle as a function of the number of negotiation slots under four different traffic scenarios.

The average number of neighbor $\mathcal{N}_i$ of the generated traffic is five, six, seven, and eight, respectively. It can be seen that the best choice of C varies when $|\mathcal{N}_i|$ varies. When C is smaller than $|\mathcal{N}_i|$, it requires more negotiation slots before a high capacity is achieved. The reason is that given a small C, a vehicle v_i would likely cast more than one neighbors into the same negotiation slot and randomly pick one to negotiate, which means that the negotiation decisions could be inconsistent among vehicles and hurts the matching efficiency per slot. This can be remedied by increasing the number of negotiation slots. On the contrary, a large C would waste many negotiation slot unassigned. As a result, it would be ideal if $C = |\mathcal{N}_i|$ as seen from Fig. 13. Since $|\mathcal{N}_i|$ varies, $C = 7$ is a good practice.

3) Effect of the Number of Neighbor Discovery Rounds K: In this experiment, we study the effect of the number of neighbor discovery rounds K. We generate traffic of different densities as set in above experiments and set the number of negotiation slots M equal to 32. In each traffic setting, we vary k from one to four with an interval of one and repeat the experiment for one hundred times.

Fig. 14 plots the cumulative density function (CDF) of OCR and ATP, respectively, obtained with different neighbor discovery rounds when the traffic density is 20 vpl. It can be seen from the figure that when $K = 3$ mmV2V achieves the best performance. The reason is that the SND protocol is a probabilistic neighbor discovery method. Using more discovery rounds will find more neighbors but also spends more time. A good tradeoff is $K = 3$, according to the observation in Section III-B, the expected ratio of identified neighbors in a single beacon is 87.5% and time overhead of SND is 2.4 ms in one beacon. Similar results are seen in other traffic scenarios.

4) Effect of the Number of Negotiation Slots M: We explore the effect of the number of negotiation slots M under different traffic densities in this experiment. We generate traffic of different densities as set in above experiments and calculate the average throughput per vehicle in the whole network with M varying from 1 to 70 with an interval of 1. We repeat experiments for 100 times and calculate the average results under each traffic density.

Fig. 15 plots the average throughput per vehicle as a function of M. It can be seen that a higher traffic density leads to a higher

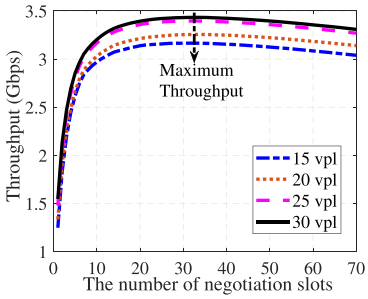

Fig. 15. Performance of DCM under different traffic densities.

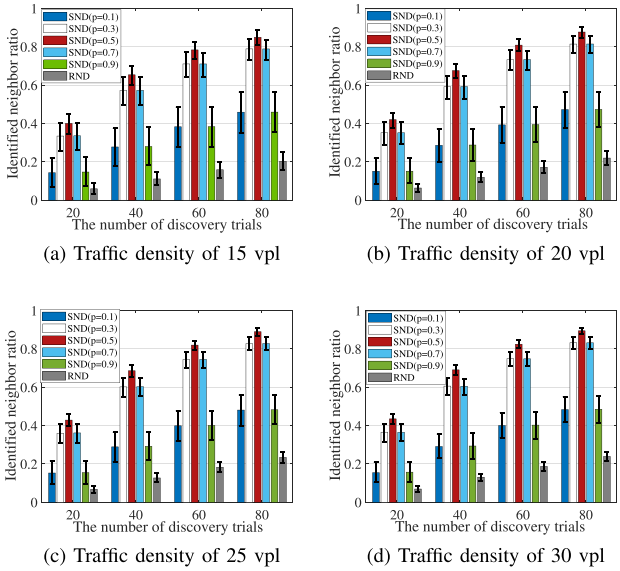

Fig. 16. Comparison of different neighbor discovery schemes.

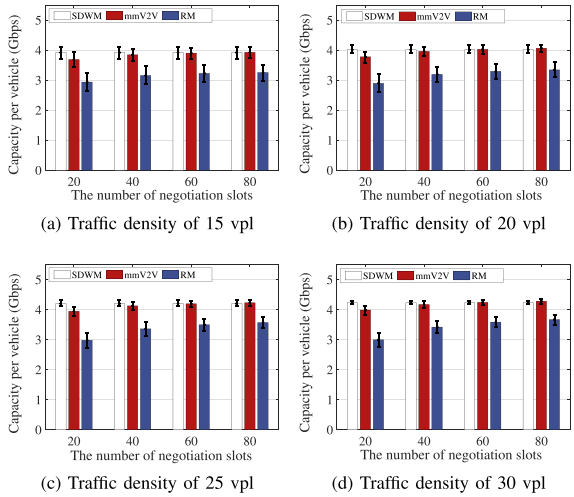

Fig. 17. Comparison of different matching schemes.

throughput per vehicle as the average link quality gets better with a shorter distance between vehicles. It can also be seen that the average throughput per vehicle reaches the maximum at certain M. It is because an insufficient M will lead to sub-optimal matching results whereas an overwhelming M wastes more time for data transmission. As a result, the maximum throughput is achieved when M equals to from 31 to 33 when the traffic density varies from 15 to 30 vpl. We take $M = 32$ as a general setting for different traffic densities.

C. Performance Comparison

1) Comparison of Different Neighbor Discovery Schemes: We first compare our SND protocol with RND in different traffic conditions. As RND does not organize neighbor discovery into synchronized rounds, we compare both schemes with the same number of individual Tx or Rx beamforming trials. In each traffic setting, we vary the number of neighbor discovery trials from 20 to 80 with an interval of 20. For SND, we vary the probability p in role selection from 0.1 to 0.9 with an interval of 0.2. We calculate the ratio of identified neighbors and repeat the experiment for one hundred times. Fig. 16 plots the ratio of identified neighbors as the function of neighbor discovery trials. It can be seen that for all traffic conditions, SND achieves the best performance when $p = 0.5$ which is consistent with our observation in Section III-B. Moreover, it can also be seen that SND can discover vast majority of neighbors after a moderate number of discovery trials and outwits RND by over three times.

2) Comparison of Different Matching Schemes: We compared our DCM protocol with other two matching algorithms, i.e., RM and SDWM. In each traffic setting, we vary the number of negotiation slots M from 20 to 80 with an interval of 20. We calculate the average communication capacity per vehicle over the whole network after a certain number of negotiation slots and repeat the experiment for one hundred times. Fig. 17 plots the communication capacity per vehicle as the function of the number of negotiation slots. It can be seen that DCM converges faster and achieves higher capacity per vehicle than RM in all traffic scenarios. Moreover, DCM can achieve similar convergence speed and capacity per vehicle compared with SDWM where vehicles have an additional broadcasting side channel.

3) Comparison of Different Overall Protocols: Finally, we compare mmV2V as a whole OHM protocol with ROP and IEEE 802.11ad in different traffic scenarios. In each setting, we set $\alpha = 30°, \beta = 12°, \theta = 15°, C = 7, K = 3$, and $M = 32$.

First, we compare three protocols in different traffic densities. In each traffic setting, vehicle performs a 200 Mbps *HRIE* task, we vary traffic density from 15 to 30 vpl with an interval of 5. Fig. 18 plots three metrics as functions of the traffic density. It can be seen that mmV2V can achieve a high average OCR of 74.7% when the traffic density is 15 vpl (i.e., the distance D between a pair of vehicle on a lane is about 66 meters). In contrast, the average OCR achieved by ROP and 802.11ad at the same traffic density are 31.9% and 46.5%, respectively. Even when the traffic density reaches 30 vpl ($D = 33$ meters), the average OCR achieved by mmV2V is 56.4%, comparing to 22.7% and 19.2% obtained by ROP and 802.11ad, respectively.

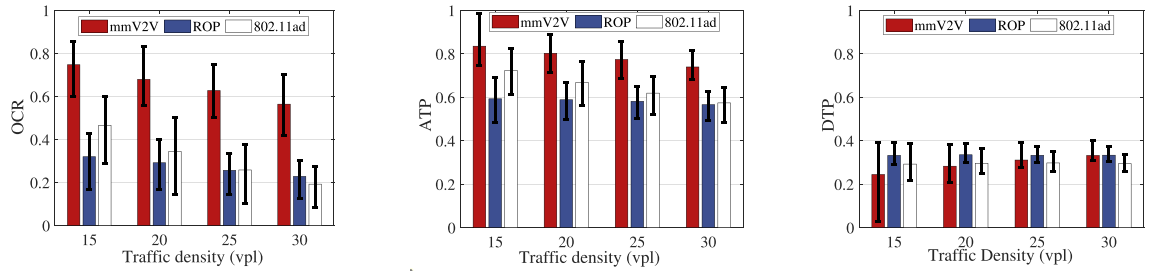

(a) OCR obtained in different traffic densities (b) ATP obtained in different traffic densities (c) DTP obtained in different traffic densities

Fig. 18. Comparison of different protocols in different traffic densities.

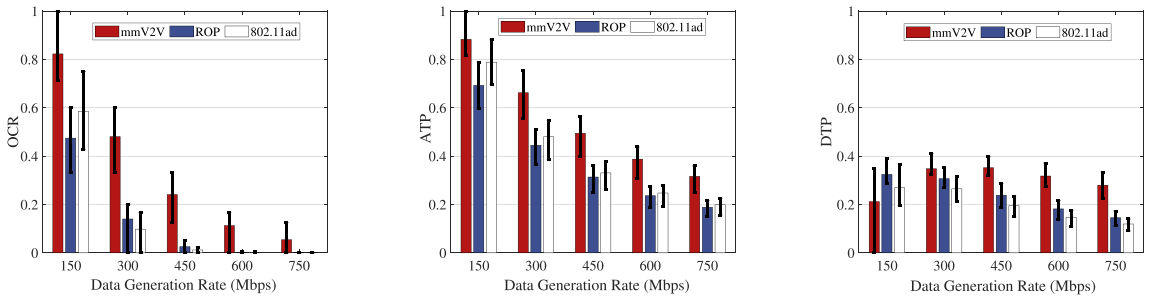

(a) OCR obtained in different data generation rates (b) ATP obtained in different data generation rates (c) DTP obtained in different data generation rates

Fig. 19. Comparison of different protocols in different data generation rates.

Furthermore, from Fig. 18(c), it can be seen that when traffic density and the corresponding workload is low, mmV2V can complete the HRIE task among most vehicles, leading to small DTP values. When the traffic density is high, mmV2V prefers to complete data exchange between vehicles with better link quality, resulting a higher DTP.

Second, we compare mmV2V with ROP and IEEE 802.11ad in different sensory data generation rates. In each setting, we set vehicle density to 20 vpl and vary sensory data generation rate of each vehicle from 150 Mbps to 750 Mbps with an interval of 150 Mbps.

Fig. 19 plots three metrics as functions of the data generation rate. It can be seen that mmV2V achieves better performance than two other protocols at all sensory data generation rates. When the sensory data generation rate is 150 Mbps, mmV2V can achieve a high average OCR of 82.3% while the average OCR achieved by ROP and 802.11ad at the same data generation rate are 47.4% and 58.6%, respectively. Even when the sensory data generation rate of each vehicle reaches 750 Mbps, mmV2V can still achieve an average ATP of 31.6%, while comparing ROP and 802.11ad can only achieve an average ATP of 18.8% and 19.9%, respectively. Furthermore, Fig. 19(c) demonstrates that when sensory data generation rate of each vehicle is low which means workload of the whole network is low, mmV2V can complete most of data exchange tasks between vehicles, leading to small DTP values.

Finally, we evaluate mmV2V and other two protocols on the highD dataset. Similarly, we vary the sensory data generation rate in the same way as above. Fig. 20 plots three metrics as functions of the data generation rate. It can be seen that mmV2V can also achieves better performance than two other protocols. When the sensory data generation rate is 150 Mbps, mmV2V can achieve a average OCR of 71.3% while the average OCR achieved by ROP and 802.11ad at the same data generation rate are 35.4% and 49.2%, respectively. When the sensory data generation rate reaches up tp 750 Mbps, mmV2V can still achieve a high ATP of 30.4%, comparing to 15.9% and 19.7% obtained by ROP and 802.11ad, respectively.

VI. Discussion

In this section, we discuss issues that mmV2V may encounter in practice.

Protocol efficiency and feasibility: The overhead of mmV2V mainly steps from the SND and the DCM schemes. With COTS mmWave hardware, the SND with three rounds of neighbor discovery takes $0.8 \times 3 = 2.4$ ms and the DCM with 32 negotiation slots takes $0.03 \times 32 = 1$ ms. Therefore, on one hand, long beacons would have high bandwidth utility. On the other hand, it is also critical for mmV2V to deal with fast movement of vehicles. Consistent neighbor distribution calls for short beacons. As a result, there is a tradeoff between the protocol efficiency and feasibility. We take beacons of 20 ms as an appropriate configuration. For instance, in the worst case where two vehicles locating in adjacent lanes of 5 meters wide move in the opposite directions, the maximum relative speed that

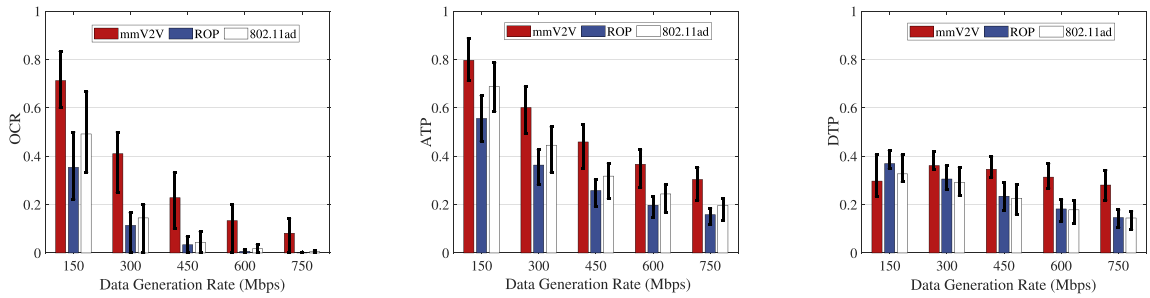

(a) OCR obtained in different data generation rates

(b) ATP obtained in different data generation rates

(c) DTP obtained in different data generation rates

Fig. 20. Comparison of different protocols on the highD trace.

will not lead to change of best beam pair in a beacon reaches 233 km/h. Meanwhile, beacons of 20 ms can achieve a relative high bandwidth utility of 83% (i.e., 16.6 ms is used for data transmission).

Probability of message collisions: Based on the SND design and the characteristic of highly directional communication of mmWave, all Tx vehicles will transmit sweep frames to the same sector at same time so that message collisions can be mostly avoided. Moreover, angle range of one sector in mmV2V is small, e.g., 15°, making the situation where two vehicles co-locate in the same sector is rare. In case two vehicles v_i and v_j co-locate in the same sector, message collisions happen only when v_i and v_j both select the same role and a third vehicle v_k in the same sector selects another role. The probability of occurring of this situation is 25% in one round of neighbor discovery. When the number of neighbor discovery rounds K equals to 3, the probability of message collision occurring in the SND is as low as $25\%^3 = 1.6\%$.

Effect of channel dynamics: Channel dynamics in traffic scenarios are mostly caused by Doppler Effect. The Doppler frequency shift f_D can be calculated as $\frac{vcos\alpha}{\lambda}$ where v is the relative speed between two vehicles, α is the angle of arrival and λ is the carrier wavelength. When the relative speed is 60 km/h and the angle of arrival is 10°, $f_D = 3.28KHZ$.

The coherence time T_c is defined as the time at which the channel correlation decreases to a predefined value R and the channel can be treated as unchanged during coherence time. T_c can be calculated as $\frac{\sqrt{1/R^4-1}}{2\pi f_D \theta^2}$ [26] where θ is the beam width of receiver which is 10° after beam refinement. When $R = 0.5$ and $f_D = 3.28KHZ$, it can be calculated that $T_c = 6$ms. In our experiments, vehicle positions and link quality are updated every 5 ms which meets the requirement of coherence time.

VII. Related Work

Traditional mmWave Networks: Beam alignment is a classic topic in researches about mmWave networks [31], [32], [33], [34], [35]. Hassanieh et al. [31] utilized multi-armed beams and proposed a hash-based algorithm to decrease the complexity of beam searching. Their result demonstrated that the best beam can be founded in a logarithmic number of measurements. Hashemi et al. [36] modeled the beam alignment problem as an online stochastic optimization problem and utilized a contextual MAB model to solve it. Their algorithm is proved to be asymptotically optimal. Haider et al. [34] calculated the best beam direction on device by tracking indicator LEDs on Wireless APs and no beam training is required. These beam alignment algorithms mainly focus on beam alignment between two nodes.

Plenty of research is done to increase the throughput and robustness of the communication in mmWave networks. Jog et al. [11] proposed a protocol called BounceNet which conduct many-to-many beam alignment between multiple APs and clients and calculate a communication combination with minimum interference. Zhang et al. [12] proposes a protocol called mmChoir to tackle the problem of blockage occuring in mmWave networks by letting multiple APs transmit to the clients simultaneously. Wei et al. [37] proposed a 60 GHz network architecture called Pia which employs pose information on mobile devices, together with a multi-AP network architecture, to achieve seamless coverage in mmWave networks. Experiment results show that BounceNet, mmChoir and Pia can increase the performance of mmWave network. However, all of these protocols are all designed for indoor scenarios and requires centralized APs.

mmWave communication in VANET: Some works utilize side-channel information to help beam alignment in VANET. Va et al. [38] utilized GPS information to aid beam prediction. Gonzalez-Prelcic et al. [39] utilized the channel information of mmWave radar to help conduct beam alignment. However these works only focus on beam alignment in VANET.

Wang et al. [2] deployed an experimental testbed consisting of one vehicle and four RSUs to enable microscopic investigation of the channel and the V2R link. From extensive measurement, they found that beam management can be handled easily if the codebook is properly designed. Moreover, highly effective spatial multiplexing can be realized with aligned transmission and reception beams. However, their work only investigates the characteristics of mmWave links in vehicular environments. Kim et al. [10] placed commercial 802.11ad products on two vehicles and conducted real-world experiments to evaluate the performance of 802.11ad in V2V communications, their results demonstrated that link quality is mainly effected by vehicle speed and distance between vehicles. However, their work only investigates the data transmission between two vehicles.

The most relevant work to our scheme is the matching scheme proposed by Perfecto et al. [40]. This work proposed a distributed

association and beam alignment scheme in mmWave VANETs, where vehicles are matched based on a utility function. However, this work mainly considers the matching strategy without considering how to efficiently schedule vehicles in a distributed network setting.

VIII. Conclusion

In this work, a fully distributed OHM scheme in vehicular networks, called mmV2V, has been proposed. In mmV2V, vehicles can efficiently discover their one-hop neighbors with directional beams. Moreover, individual vehicles can collectively make a communication schedule to achieve appealing network throughput. We have implemented a 60 GHz testbed to verify the feasibility of mmV2V. From our implementation, mmV2V is a lightweight and fully distributed scheme, requiring the minimal hardware. We have conducted extensive simulations and the results demonstrate that mmV2V can achieve a high completion ratio in rigid OHM tasks under various traffic conditions.

References

[1] G. Luo, Q. Yuan, J. Li, S. Wang, and F. Yang, "Artificial intelligence powered mobile networks: From cognition to decision," *IEEE Netw.*, vol. 36, no. 3, pp. 136–144, May/Jun. 2022.

[2] S. Wang, J. Huang, and X. Zhang, "Demystifying millimeter-wave V2X: Towards robust and efficient directional connectivity under high mobility," in *Proc. 26th Annu. Int. Conf. Mobile Comput. Netw.*, 2020, Art. no. 51.

[3] K. Huang, B. Shi, X. Li, X. Li, S. Huang, and Y. Li, "Multi-modal sensor fusion for auto driving perception: A survey," 2022, *arXiv:2202.02703*.

[4] G. Luo et al., "EdgeCooper: Network-aware cooperative LiDAR perception for enhanced vehicular awareness," *IEEE J. Sel. Areas Commun.*, vol. 42, no. 1, pp. 207–222, Jan. 2024.

[5] G. Luo et al., "Software-defined cooperative data sharing in edge computing assisted 5G-VANET," *IEEE Trans. Mobile Comput.*, vol. 20, no. 3, pp. 1212–1229, Mar. 2021.

[6] F. Ahmad, H. Qiu, R. Eells, F. Bai, and R. Govindan, "CarMap: Fast 3D feature map updates for automobiles," in *Proc. USENIX Conf. Networked Syst. Des. Implementation*, 2020, pp. 1063–1081.

[7] W. Yi, Y. Liu, Y. Deng, A. Nallanathan, and R. W. Heath, "Modeling and analysis of MmWave V2X networks with vehicular platoon systems," *IEEE J. Sel. Areas Commun.*, vol. 37, no. 12, pp. 2851–2866, Dec. 2019.

[8] H. Qiu, F. Ahmad, F. Bai, M. Gruteser, and R. Govindan, "AVR: Augmented vehicular reality," in *Proc. 16th Annu. Int. Conf. Mobile Syst. Appl. Services*, 2018, pp. 81–95.

[9] M. H. C. Garcia et al., "A tutorial on 5G NR V2X communications," *IEEE Commun. Surv. Tut.*, vol. 23, no. 3, pp. 1972–2026, Third Quarter 2021.

[10] W. Kim, "Experimental demonstration of MmWave vehicle-to-vehicle communications using IEEE 802.11ad," *Sensors*, vol. 19, no. 9, 2019, Art. no. 2057.

[11] S. Jog, J. Wang, J. Guan, T. Moon, H. Hassanieh, and R. R. Choudhury, "Many-to-many beam alignment in millimeter wave networks," in *Proc. USENIX Conf. Networked Syst. Des. Implementation*, 2019, pp. 783–800.

[12] D. Zhang, M. Garude, and P. H. Pathak, "mmChoir: Exploiting joint transmissions for reliable 60GHz MmWave WLANs," in *Proc. 18th ACM Int. Symp. Mobile Ad Hoc Netw. Comput.*, 2018, pp. 251–260.

[13] H. A. Omar, W. Zhuang, and L. Li, "VeMAC: A TDMA-Based MAC protocol for reliable broadcast in VANETs," *IEEE Trans. Mobile Comput.*, vol. 12, no. 9, pp. 1724–1736, Sep. 2013.

[14] Y. Cai, H. Zhu, S. Chang, X. Wang, J. Shen, and M. Guo, "PeerProbe: Estimating vehicular neighbor distribution with adaptive compressive sensing," *IEEE/ACM Trans. Netw.*, vol. 30, no. 4, pp. 1703–1716, Aug. 2022.

[15] I. Holyer, "The np-completeness of edge-coloring," *SIAM J. Comput.*, vol. 10, no. 4, pp. 718–720, 1981.

[16] S. Jayaprakasam, X. Ma, J. W. Choi, and S. Kim, "Robust beam-tracking for mmWave mobile communications," *IEEE Commun. Lett.*, vol. 21, no. 12, pp. 2654–2657, Dec. 2017.

[17] "USRP N210 Kit," 2023. [Online]. Available: https://www.ettus.com/all-products/un210-kit/

[18] "SIVERS EVK06002 evaluation kit," [Online]. Available: https://www.sivers-semiconductors.com/sivers-wireless/evaluation-kits/

[19] J. Wildman, P. H. J. Nardelli, M. Latva-aho, and S. Weber, "On the joint impact of beamwidth and orientation error on throughput in directional wireless Poisson networks," *IEEE Trans. Wireless Commun.*, vol. 13, no. 12, pp. 7072–7085, Dec. 2014.

[20] "VEhicular networking universal simulator," 2023. [Online]. Available: http://lion.sjtu.edu.cn/project/projectDetail?id=17

[21] R. Krajewski, J. Bock, L. Kloeker, and L. Eckstein, "The high D dataset: A drone dataset of naturalistic vehicle trajectories on German highways for validation of highly automated driving systems," in *Proc. 21st Int. Conf. Intell. Transp. Syst.*, 2018, pp. 2118–2125.

[22] A. Yamamoto, K. Ogawa, T. Horimatsu, A. Kato, and M. Fujise, "Path-loss prediction models for intervehicle communication at 60GHz," *IEEE Trans. Veh. Technol.*, vol. 57, no. 1, pp. 65–78, Jan. 2008.

[23] "*IEEE Standard for Information technology–Telecommunications and information exchange between systems–Local and metropolitan area networks–Specific requirements-Part 11: Wireless LAN Medium Access Control (MAC) and Physical Layer (PHY) Specifications Amendment 3: Enhancements for Very High Throughput in the 60GHz Band*," IEEE Std 802.11ad-2012 (Amendment to IEEE Standard 802.11–2012, as amended by IEEE Standard 802.11ae-2012 and IEEE Standard 802.11aa- 2012), pp. 1–628, 2012.

[24] H. A. Mahmoud and H. Arslan, "Error vector magnitude to SNR conversion for nondata-aided receivers," *IEEE Trans. Wireless Commun.*, vol. 8, no. 5, pp. 2694–2704, May 2009.

[25] P. Zhou, X. Fang, Y. Fang, Y. Long, R. He, and X. Han, "Enhanced random access and beam training for millimeter wave wireless local networks with high user density," *IEEE Trans. Wireless Commun.*, vol. 16, no. 12, pp. 7760–7773, Dec. 2017.

[26] V. Va and R. W. Heath, "Basic relationship between channel coherence time and beamwidth in vehicular channels," in *Proc. IEEE 82nd Veh. Technol. Conf.*, 2015, pp. 1–5.

[27] 3GPP, "Study on enhancement of 3GPP support for 5 G V2X services (Release 16)," Technical Report (TR) 22.886, 3rd Generation Partnership Project, 2018. V16.2.0.

[28] J. Ning, T.-S. Kim, S. V. Krishnamurthy, and C. Cordeiro, "Directional neighbor discovery in 60 GHz indoor wireless networks," *Perform. Eval.*, vol. 68, no. 9, pp. 897–915, 2011..

[29] J. Hoepman, "Simple distributed weighted matchings," 2004, *arXiv:cs/0410047*.

[30] B. Coll-Perales, M. Gruteser, and J. Gozalvez, "Evaluation of ieee 802.11ad for mmWave V2V communications," in *Proc. IEEE Wireless Commun. Netw. Conf. Workshops*, 2018, pp. 290–295.

[31] H. Hassanieh, O. Abari, M. Rodriguez, M. Abdelghany, D. Katabi, and P. Indyk, "Fast millimeter wave beam alignment," in *Proc. ACM SIGCOMM Conf.*, 2018, pp. 432–445.

[32] M. E. Rasekh, Z. Marzi, Y. Zhu, U. Madhow, and H. Zheng, "Noncoherent MmWave path tracking," in *Proc. 18th Int. Workshop Mobile Comput. Syst. Appl.*, 2017, pp. 13–18.

[33] N. J. Myers, A. Mezghani, and R. W. Heath, "Swift-link: A compressive beam alignment algorithm for practical mmWave radios," *IEEE Trans. Signal Process.*, vol. 67, no. 4, pp. 1104–1119, Feb. 2019.

[34] M. K. Haider, Y. Ghasempour, D. Koutsonikolas, and E. W. Knightly, "LiSteer: MmWave beam acquisition and steering by tracking indicator LEDs on wireless APs," in *Proc. 24th Annu. Int. Conf. Mobile Comput. Netw.*, 2018, pp. 273–288.

[35] J. Palacios, D. Steinmetzer, A. Loch, M. Hollick, and J. Widmer, "Adaptive codebook optimization for beam training on off-the-shelf IEEE 802.11ad devices," in *Proc. 24th Annu. Int. Conf. Mobile Comput. Netw.*, 2018, pp. 241–255.

[36] M. Hashemi, A. Sabharwal, C. Emre Koksal, and N. B. Shroff, "Efficient beam alignment in millimeter wave systems using contextual bandits," in *Proc. IEEE Conf. Comput. Commun.*, 2018, pp. 2393–2401.

[37] T. Wei and X. Zhang, "Pose information assisted 60 GHz networks: Towards seamless coverage and mobility support," in *Proc. 23rd Annu. Int. Conf. Mobile Comput. Netw.*, 2017, pp. 42–55.

[38] V. Va, X. Zhang, and R. W. Heath, "Beam switching for millimeter wave communication to support high speed trains," in *Proc. IEEE 82nd Veh. Technol. Conf.*, 2015, pp. 1–5.

[39] N. González-Prelcic, R. Méndez-Rial, and R. W. Heath, "Radar aided beam alignment in MmWave V2I communications supporting antenna diversity," in *Proc. Inf. Theory Appl. Workshop*, 2016, pp. 1–7.

[40] C. Perfecto, J. Del Ser, and M. Bennis, "Millimeter-wave V2V communications: Distributed association and beam alignment," *IEEE J. Sel. Areas Commun.*, vol. 35, no. 9, pp. 2148–2162, Sep. 2017.

Jiangang Shen (Member, IEEE) received the BS degree from Shanghai Jiaotong University, in 2019. He is currently working toward the postgraduate degree with the Department of Computer Science and Technology, Shanghai Jiaotong University, Shanghai. His research interests include Internet of Things and wireless network.

Hongzi Zhu (Member, IEEE) received the BS and ME degrees in computer science from Jilin University, China, in 2001 and 2004, respectively, and the PhD degree in computer science from Shanghai Jiao Tong University, in 2009. He was a postdoctoral fellow with the Department of Computer Science and Engineering, Hong Kong University of Science and Technology, and the Department of Electrical and Computer Engineering, University of Waterloo, in 2009 and 2010, respectively. He is a professor with the Department of Computer Science and Engineering, Shanghai Jiao Tong University. His research interests include Internet of Things and mobile computing. He received the Best Paper Award from IEEE GLOBECOM 2016. He is an associate editor for *IEEE Transactions on Vehicular Technology* and *IEEE Internet of Things Journal*. He is a IEEE VTC distinguished lecturer.

Yunxiang Cai (Member, IEEE) received the BS degree in physics from the Ocean University of China, in 2018. He is currently working toward the PhD degree with the Department of Computer Science and Technology, Shanghai Jiao Tong University, under the supervision of Prof. Hongzi Zhu. His research interests include vehicular ad hoc networks and mobile computing.

Shan Chang (Member, IEEE) received the PhD degree in computer software and theory from Xian Jiaotong University, in 2013. From 2009 to 2010, she was a visiting scholar with the Department of Computer Science and Engineering, Hong Kong University of Science and Technology. She was also a visiting scholar with the BBCR Research Lab, University of Waterloo, from 2010 to 2011. She is now an associate professor with the Department of Computer Science and Technology, Donghua University, Shanghai. Her research interests include security and privacy in mobile networks and sensor networks.

Haibin Cai (Member, IEEE) received the BEng and MS degrees in computer science and technology from the National University of Defense Technology, China, in 1997 and 2004, respectively, and the PhD degree in control theory and control engineering from the Donghua University, Shanghai, China, in 2008. He is currently a professor with the East China Normal University. His research interests include trusted AI, intelligent perception, distributed computing, and trustworthy computing.

Bangzhao Zhai (Member, IEEE) received the BS degree in information science and engineering from Southeast University, Nanjing, China, in 2015. He is currently working toward the PhD degree with the Wireless Networking and Artificial Intelligence Laboratory, Shanghai Jiao Tong University, Shanghai, China. His research interests include B5G/6 G networks, millimeter-wave (mmWave) communications, terahertz (THz) communications, and joint communication and sensing systems.

Xudong Wang (Fellow, IEEE) received the PhD degree in electrical and computer engineering from the Georgia Institute of Technology in 2003. He is currently the John Wu and Jane Sun chair professor in engineering with the UM-SJTU Joint Institute, Shanghai Jiao Tong University. He is also an affiliate professor with the Department of Electrical and Computer Engineering, University of Washington. His research interests include wireless communication networks, distributed machine learning, and joint communications and sensing. He was a voting member of IEEE 802.11 and 802.15 Standard Committees. He was the TPC co-chair of the 32nd International Conference on Information Networking. He was the Demo co-chair of ACM MOBIHOC 2006. He served as an associate editor for *IEEE Transactions on Mobile Computing* and *IEEE Transactions on Vehicular Technology*. He was also a guest editor of several international journals.

Minyi Guo (Fellow, IEEE) received the BS and ME degrees in computer science from Nanjing University, China in 1982 and 1986, respectively. He is a chair professor with the Department of Computer Science and Engineering, Shanghai Jiao Tong University (SJTU), China, and was the department head from 2009 to 2019. His present research interests include parallel/distributed computing, compiler optimizations, Big Data and cloud computing. He received 7 best/highlight paper awards from international conferences including ALSPOS 2017 and ICCD 2018. He is now editor-in-chief of *IEEE Transactions on Sustainable Computing*, and on the editorial board of *IEEE Transactions on Parallel and Distributed Systems*, *IEEE Transactions on Cloud Computing* and *Journal of Parallel and Distributed Computing*. He is a fellow of CCF, and a distinguished member of ACM.